Inelastic light scattering from density fluctuations in dilute gases. The kinetic-hydrodynamic transition in a monatomic gas*

Noel A. Clark

Gordon McKay Laboratory, Division of Engineering and Applied Physics, Harvard University, Cambridge, Massachusetts 02138

(Received 18 February 1975)

The number-density fluctuation spectrum, $S_n(\vec{K},\omega)$, of xenon has been studied in the dilute-gas limit. Spectra of He-Ne laser light scattered through an angle of 10.58° at room temperature were measured for pressures ranging from 0.02 to 0.6 atm. Over this range $S_n(\vec{K},\omega)$ evolves from the Gaussian kinetic form to three peaked hydrodynamic form. Measured spectra were used to evaluate various kinetic and hydrodynamic calculations of $S_n(\vec{K},\omega)$ through this transition. Spectra obtained from the Boltzmann equation using the Gross-Jackson kinetic modeling procedure, for both Maxwell and hard-sphere intermolecular potentials, are in excellent agreement with the measurements. Among the hydrodynamic theories tested only the generalized hydrodynamics of Selwyn and Oppenheim satisfactorily provides the initial nonhydrodynamic corrections to the Navier-Stokes equations.

I. INTRODUCTION

In recent years the use of time-dependent correlation functions to characterize the dynamical properties of condensed systems has developed extensively. Previous work has been concerned primarily with the analysis of neutron scattering experiments and molecular dynamics calculations in liquids. This focus on the liquid state may be contrasted to the earlier developments of statistical physics which were directed primarily at understanding the dilute-gas limit. However, the use of neutron scattering to probe liquid dynamics has also generated some interest in time dependent correlation functions in dilute systems. Although neutron scattering is not feasible in the dilute limit, the calculation of correlation functions is simpler than at finite densities and in some cases exact. This was the motivation for the theoretical study of density fluctuations in a dilute gas and their relation to neutron scattering in liquids.[1] The inapplicability of neutron scattering to dilute systems led to the consideration of alternative experimental techniques. In 1966, Nelkin and Yip pointed out that in a typical gas at STP a light scattering experiment could probe density fluctuations of a wavelength, λ, comparable to l, the mean free path between collisions, and that by changing scattering angle or gas density either the long-wavelength (hydrodynamic, $l \ll \lambda$) or short-wavelength (kinetic, $l \gg \lambda$) limit could be conveniently reached.[2] The utility of inelastic light scattering in probing the kinetic-hydrodynamic transition in the dilute gas limit was demonstrated shortly thereafter by Greytak and Benedek.[3] However, thorough quantitative interpretation of these and other light scattering data[4,5] in dilute gases was limited by experimental difficulties.

In this paper[6] we report the first systematic light-scattering study of the kinetic-hydrodynamic transition in a monatomic gas. We use our results to evaluate various microscopic and hydrodynamic calculations of density fluctuation spectra. We begin by relating the density fluctuation and scattered light spectra. This is followed by a qualitative description of the evolution of the density fluctuation spectrum through the kinetic-hydrodynamic transition, and a discussion of the various calculations. The details, results, and discussion of the present experiments complete the paper.

II. THEORY

A. Basics

The essential geometry is typical of Brillouin scattering experiments. Collimated monochromatic light of wave vector $\vec{k}_i$ is incident on the sample. Light scattered through an angle Θ of wave vector $\vec{k}_s$ is collected and frequency analyzed. The power spectrum of the scattered electric field, about the incident frequency ω_i, $S(\vec{K}, \omega - \omega_i)$, is proportional to the power spectrum of those fluctuations in number density which have wave vector $\vec{K} = \vec{k}_s - \vec{k}_i$. That is,[7]

$$S(\vec{K},\omega - \omega_i) \propto S_n(\vec{K},\omega) \equiv \int\int d^3r\, d\tau\, e^{i\vec{K}\cdot\vec{r} - \omega\tau} \frac{\langle \delta n(\vec{r},\tau)\delta n(0,0)\rangle}{n_0}, \tag{1}$$

where $\delta n(\vec{r}, t)$ is the fluctuation from the average number density, n_0, at the point $(\vec{r}, t)$, and $\langle\rangle$ denotes an ensemble average. The scattered light spectrum then provides a direct measurement of the density fluctuation spectrum at a wavelength $\lambda = 2\pi/K$. Since a dilute gas is isotropic $S_n(\vec{K},\omega)$

depends only on $K = |\vec{K}|$ where $K = 2k_i \sin\frac{1}{2}\Theta$.

The density fluctuation spectrum of a dilute gas undergoes a dramatic change through the kinetic-hydrodynamic transition. The evolution of $S_n(K,\omega)$, calculated for a gas of Maxwell molecules, is shown in Fig. 1. We have plotted $S(x,y)$, using a dimensionless frequency parameter $x = \omega/\Delta\omega$, where

$$\Delta\omega = 2^{1/2}Kv_0 \equiv 2^{1/2}K(k_BT/m)^{1/2}. \quad (2)$$

Here k_B is the Boltzmann constant, T the absolute temperature, and m the particle mass. The general form of the spectrum is determined by the uniformity parameter $y \sim 1/Kl$, which increases in the direction of the hydrodynamic regime. Since a gas of point particles has the single characteristic length, l, the wave vector K appears in the spectrum only as Kl. Furthermore the spectrum $S_n(K,\omega)$ is a function of x and y only $[S(x,y)]$. This scaling property of the density fluctuation spectrum was first discussed by Nelkin.[8]

In the kinetic limit, particles undergo few collisions over the length $1/K$ so the spectrum may be calculated assuming that the scattered light is Doppler shifted by molecules moving along straight lines with the equilibrium Gaussian Maxwell velocity distribution. The resulting $S_n(K,\omega)$ is Gaussian, falling to $1/e$ at $\omega = \sqrt{2}\,kv_0$ $(x = 1)$. For xenon gas at room temperature with incident light of wavelength $\lambda_i = 6328$ Å and scattering angle $\Theta = 10.6°$, one finds $\Delta\omega/2\pi = \sqrt{2}\,Kv_0/2\pi \cong 56$ MHz.

As y increases $S(x,y)$ develops three distinct peaks,[9] one located at $x = 0$ and a pair symmetric about $x = 0$ located at $x \cong \pm\sqrt{\frac{5}{6}}$. These peaks indicate the prevalence of two well-defined kinds of fluctuations (modes) in $S(x,y)$ at large y. The widths Δx_i of the peaks are comparable and vary as $1/y$ $(\Delta x_i \sim 1/y)$. Since the width of a peak is the decay rate for the fluctuations producing it, the decay rates for the two kinds of fluctuations contributing to $S(x,y)$ approach zero in the $y \to \infty$ limit. This kind of behavior has been termed hydrodynamic and is a direct consequence of the Euler conservation laws for particle number density, momentum density, and energy density. The two hydrodynamic modes of a simple fluid may be characterized as entropy fluctuations at constant pressure (heat flow), giving rise to the central peak, and pressure fluctuations at constant entropy (adiabatic sound propagation), giving rise to the shifted peaks.[10]

B. Hydrodynamic theories

Atoms in a gas travel a finite distance in space (l) and time (τ_c) between interatomic collisions. As a result, collisions are not perfectly efficient at maintaining local thermodynamic equilibrium in a fluctuation having finite wave vector (K) and frequency (ω). The object of a hydrodynamic theory is to account for the observable effects of the resulting deviation from local equilibrium. In the limits $Kl \ll 1$ and $\omega\tau_c \ll 1$ $(y \gg 1$ and $x \ll y)$ the deviation from local thermodynamic equilibrium is small and may be dealt with phenomenologically (Navier-Stokes hydrodynamic and Fourier heat-conduction equations). This is the "hydrodynamic" regime. For $y \lesssim 1$ or $x \gtrsim y$ however this approach fails and one must resort to obtaining a more general hydrodynamic description from the Boltzmann equation (BE), such as in the Chapman-Enskog procedure (CEP) or the more recent generalized hydrodynamic theories. These methods attempt to evaluate systematically small deviations from hydrodynamics for $y \gtrsim 1$. In this paper we use experimental spectra to determine the range of validity of the hydrodynamics and the success with which the more general theories supply the first "nonhydrodynamic" corrections. In particular, the theories which we have tested are (i) the hydrodynamic approximation: (a) Exact solution (NS), (b) Kadanoff-Martin (KdM) approximation, (c) three Lorentzian (3L) approximation; (ii) the Burnett (B) approximation; (iii) the Selwyn generalized hydrodynamic theory: (a) Exact (SE), (b) approximate (SA). We now discuss each of these briefly.

The hydrodynamic equations in the Navier-Stokes approximation are the first nontrivial set of hierarchy of hydrodynamic equations obtained from the Boltzmann equation via the CEP or generalized hydrodynamics. These equations are local in space and time and involve energy and momentum fluxes which are proportional to first spatial derivatives of temperature and velocity. They have been solved exactly for $S_n(K,\omega)$ by Mountain.[10] An approximate Navier-Stokes solution for $S_n(K,\omega)$ has been obtained by Kadanoff and Martin[11] and is included in the comparison. We have also included the three Lorentzian form of $S_n(K,\omega)$, since all of the hydrodynamic calculations reduce to this form as $y \to \infty$: (i) the peaks in $S_n(K,\omega)$ become Lorentzian, the central peak having a half-width at half-height (HWHH) in ω of $\Gamma_C = \Lambda K^2/n_0c_p$, and the shifted (Brillouin) peaks having a HWHH of

$$\Gamma_B = \frac{1}{2}\left[\frac{4\eta}{3mn_0} + \left(1 - \frac{1}{\gamma}\right)\frac{\Lambda}{n_0c_v}\right]K^2;$$

(ii) the shifted peaks are located at $\pm Kc_0 = \pm K(k_BT\gamma/m)^{1/2}$, where c_0 is the adiabatic sound speed; (iii) the ratio of total central intensity I_C to total shifted intensity I_B is $I_C/I_B = \gamma - 1$. Here Λ is thermal conductivity, c_p the heat capacity per particle at constant pressure, η the shear vis-

cosity, and $\gamma = c_p/c_v$.

Carrying the CEP to the next higher order [i.e., retaining deviations from local equilibrium of order $(l\,\partial/\partial x)^2 \sim 1/y^2$] produces the Burnett equations, which are also local but involve fluxes proportional to second as well as first spatial derivatives. Ranganathan and Nelkin have calculated $S_n(K,\omega)$ in the Burnett approximation for a gas of Maxwell molecules.[12]

More recently the methods of generalized hydrodynamics have been employed by Selwyn and Oppenheim in the calculation of $S_n(K,\omega)$ for a monatomic gas.[13] Here linear response theory is applied to the Liouville equation to develop an expansion in $\vec{K}$ about $\vec{K}=0$ of the dynamical matrix $\vec{M}_{ij}(\vec{K},\omega)$ which determines the space-time evolution of correlation functions of the conserved variables of the system. With this expansion the effects of nonhydrodynamic (microscopic) modes are accounted for to a selected order in $\vec{K}$. For $\vec{K}=0$ one finds $M_{ij}(\vec{K},\omega)=0$ and the Euler conservation equations are obtained. Keeping terms in M_{ij} linear in $\vec{K}$ results in the Navier-Stokes equations. The next higher order yields spatially and temporally nonlocal equations which Selwyn has solved for $S_n(K,\omega)$ of a gas of Maxwell molecules. We include in our comparison Selwyn's exact $S_n(K,\omega)$ as well as an approximate form which he obtained by partial-fraction expansion of the exact form.

C. Kinetic theories

In addition to hydrodynamic calculations a number of direct solutions of the Boltzmann equation (BE) for $S_n(K,\omega)$ have been attempted. A rigorous basis for obtaining $S_n(K,\omega)$ from the BE was developed from the Liouville equation by Van Leeuwen and Yip.[14] Because of approximations involved in the modeling and solution of the BE, initial efforts were only qualitatively successful and are not discussed here.[15] These efforts did, however, lead to the calculation of Sugawara, Yip, and Sirovich[16] who used the Gross-Jackson kinetic modeling procedure[17] to solve the BE. Kinetic modeling, an extension of the methods of Wang Chang and Uhlenbeck, involves expansion of the BE distribution function in a complete orthonormal set of functions $\phi_i(\vec{v})$ which are eigenfunctions of the BE collision operator. With appropriate initial conditions an infinite set of linear equations are obtained which are solved by replacing the eigenvalues of the collision operator, λ_i, by the value λ_M for $i > M$, where M is an arbitrary cutoff. This method, because it preserves all velocity moments of the distribution function, allows convergence at finite M in both the kinetic and hydrodynamic limits. Spectra calculated for successive orders of approximation, M, converge when M is sufficiently large.[16] The result is an apparently exact solution of the BE for the density fluctuation spectrum $S(x,y)$ for all values of x and y. This method has been applied to both Maxwell $(1/r^4)$ and hard-sphere molecules to evaluate the effect of intermolecular potential on $S(x,y)$. The spectra calculated for these two choices of potential are nearly identical, differing at most by only a few percent for a given (x,y). Figure 1 shows $S(x,y)$ for a gas of Maxwell molecules calculated using the kinetic model with $M=21$, at which convergence of $S(x,y)$ to within 1% of its limiting form is obtained. For a discussion of the convergence of the kinetic model procedure see Ref. 16.

Density fluctuation spectra calculated in the dilute gas limit are functions of two parameters: the reduced frequency x (see Eq. 2) and the wave vector K which appears only as the single additional parameter $y = 1/Kl$. The reduced frequency x is determined uniquely by experimental conditions. For y to be uniquely specified, however, the theoretical model used to obtain the transport coefficients η and Λ must correctly provide the Eucken ratio $E = m\Lambda/\eta c_v$ of the gas under study. Since both η and Λ are measurable, either may be used to specify y.

From either the kinetic model (KM)[16] or CEP[18] we find

$$y \equiv (\sqrt{2}/3)(mn_0v_0/\eta K) \tag{3}$$

or

$$y \equiv \begin{Bmatrix} 1.00 \\ 1.02 \end{Bmatrix} \frac{5}{3\sqrt{2}} \frac{n_0 v_0 c_v}{\Lambda K} \begin{Bmatrix} \text{Maxwell} \\ \text{hard sphere} \end{Bmatrix}. \tag{4}$$

If Eqs. 3 and 4 are to yield a unique value of y then the measured Eucken ratio must be that predicted by the KM and CEP for the particular intermolecular potential employed. For the Maxwell and hard-sphere potentials both the KM and the CEP yield

$$\frac{\Lambda}{\eta c_v} = \begin{cases} 2.50 & \text{Maxwell} \\ 2.515 & \text{hard sphere} \end{cases} \tag{5}$$

We have compared measured Eucken ratios of real gases to these values. Eucken ratios were calculated from the measured viscosity[19] and thermal conductivity[20] of the simple gases xenon, krypton, argon, and neon at 25°C. The ideal gas value of c_v was used in all cases.[21] The results are summarized in Table I. Measured values of E at $T = 25$°C and $p = 1$ atm were found to be $E = 2.50$ within experimental error. The determination of y therefore for either the Maxwell or hard-sphere potential is unambiguous at $T = 25$°C for

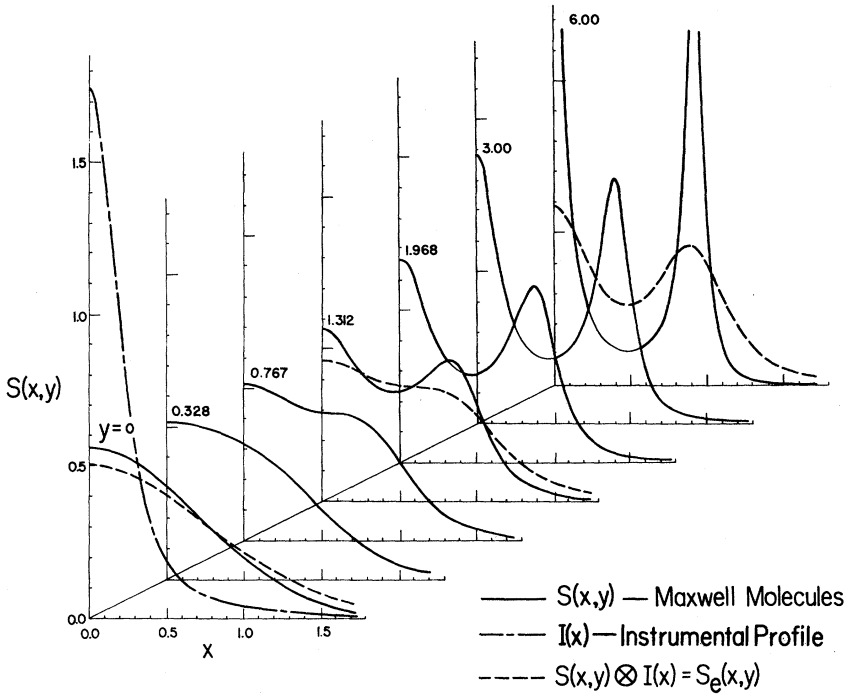

FIG. 1. Exact solution of the Boltzmann equation for the density fluctuation spectrum of a dilute gas of Maxwell molecules. Effect of the convolution of $S(x,y)$ with the instrumental profile $I(x)$ is indicated for several values of y.

these gases. Since in xenon measurements of η are more accurate we shall use Eq. 3 to determine y. Once x and y are determined there are no adjustable parameters in the theoretical spectra.

D. Calculated spectra

To facilitate the comparison of experimental and theoretical spectra we have calculated and tabulated the various hydrodynamic and kinetic spectra $S(x,y)$ in terms of the dimensionless variables x and y with $S(x,y)$ normalized to unity in x: $\int_{-\infty}^{\infty} dx\, S(x,y) = 1$. Analytic expressions for the hydrodynamic spectra are given in Appendix A. The hydrodynamic spectra S_{NS}, S_{KdM}, S_{3L}, S_B, S_{SE}, and S_{SA} were calculated for $|x| \leq 3.2$ and $y = 0.767$, 1.312, 3.00, 4.65, and 6.00. Spectra were calculated from the KM approximation[16] for $M = 21$, $|x| \leq 3.2$, and $y = 0$, 0.1, 0.328, 0.5, 0.767, 1.312, 1.968, 3.00, 4.65, and 6.00 for Maxwell molecules and for hard-sphere molecules at $y = 0.328$, 0.767, 1.312, 1.968, 3.00, and 6.00. Point spacings required for accurate numerical convolution with the instrumental profile were $\Delta x = 0.025$ for $y < 3$ and $\Delta x = 0.006\,25$ for $y > 3$. In Appendix B, the hydrodynamic and KM spectra are tabulated for a selected set of (x,y) values. In addition, Table III gives the location and height of the Brillouin peaks for the various calculations.

E. Experimental conditions

Our goal in these experiments was to study $S_n(K,\omega)$ in a simple gas under conditions where the Boltzmann equation would be expected to work, i.e., where imperfect gas corrections are negligible. With this as the primary consideration the choice of xenon at a scattering angle $\Theta = 10.6°$ was arrived at. This choice presents the following disadvantages and advantages.

Disadvantages. (i) In the forward direction ($\Theta \sim 0°$) the scattered light spectrum is relatively narrow, placing more stringent requirements on the frequency stability and spectral width of the incident light than at larger angles. (ii) Spectral distortion due to the finite range of $\vec{K}$ vectors participating in the scattering process is most serious in the forward direction. This problem was overcome by the use of conical collection optics.[3] (iii) Stray light tends to be stronger at small scattering angles. These experimental problems will be discussed in the next section.

Advantages. (i) As the scattering angle nears the forward ($\Theta \sim 0°$) direction the illuminated volume from which one can collect scattered light into a

TABLE I. Thermal conductivity, shear viscosity, and Eucken ratio of simple gases at 25 °C and 1 atm.

	Λ (kcal/sec cm °C) (Ref. 20)	η (μPoise) (Ref. 19)	E
Xe	1.316 ± 1%	231.02 ± 0.06%	2.509 ± 0.025
Kr	2.265 ± 1%	253.22 ± 0.06%	2.515 ± 0.025
Ar	4.22 ± 0.5%	226.38 ± 0.04%	2.498 ± 0.012
Ne	11.60 ± 0.5%	317.30 ± 0.05%	2.503 ± 0.012

spectrometer increases. (ii) The spectrum is sufficiently narrow that a spherical Fabry-Perot interferometer (FPS) may be used. The FPS has very stable instrumental transmission characteristics, obviating the need for frequent measurement of the instrumental profile. (iii) The kinetic-hydrodynamic transition occurs over the density range from $n_0 \sim 0.16$ amagat ($p \sim 0.014$ atm, $y \sim 0.1$) to $n_0 \sim 0.7$ amagat ($p \sim 0.6$ atm, $y \sim 5$). At these densities the following conditions are satisfied in our experiments: (a) time intervals which are probed ($\gtrsim 10^{-9}$ sec) are long compared to the duration of interatomic collisions ($\sim 10^{-11}$ sec if we include the formation of dimers). (b) Lengths probed ($\sim 6\times 10^4$ Å) are long compared to the range of molecular interaction (~ 4 Å). (c) The atomic volume, v^*, is small compared to the volume available per atom in the gas, $1/n_0$, ($n_0 v^* < 5\times 10^{-4}$).

Van Leeuwen and Yip have shown[14] that the linearized BE should correctly provide the density fluctuation spectrum when conditions (a) and (b) are in force. Condition (c) indicates the validity of the assumptions, implicit in the BE, that there are no static positional correlations in the gas and that only binary collisions occur. That is, static correlations and three-particle collisions lead to (imperfect gas) corrections of the thermodynamic and transport parameters respectively which are on the order of $n_0 v^*$. For the BE to be applicable then, $n_0 v^*$ must be small enough so that modifications of the spectra due to imperfect gas corrections are too small to be observed. The most serious correction is that to the adiabatic sound speed c_0, which determines the Brillouin peak location and for which we have the following virial expansion[22]

$$c_0 = (5k_B T/3\pi)^{1/2}\{1 - 0.0043[n_0 \text{ (amagat)}]\}, \quad (6)$$

where $(5k_B T/3m)^{1/2}$ is the BE (ideal gas) value. For our experiments ($n_0 \lesssim 0.7$ amagat) the correction to c_0 is $\lesssim -0.4\%$ and is not observable. Similar results are found for the other spectral corrections. Thus at the highest density studied, where the corrections are most serious, condition (c) is satisfied to such an extent that deviations of the parameters which determine the spectrum ($\eta, \Lambda, c_0, c_p, c_v, \gamma$) from their ideal gas—BE values are not observable. In satisfying conditions (a)–(c), then, obvious reasons for the failure of the BE are eliminated.

III. EXPERIMENTAL DETAILS

A. Introduction

A block diagram of the experimental apparatus is shown in Fig. 2. The light source is a He-Ne laser producing 10–15 mW of optical power in a single frequency-stabilized TEM_{00} mode. Light from the laser is pinhole spatial filtered and weakly focused into the scattering cell containing the gas under study. The incident beam passes out of the scattering cell through holes in the conical lens and mirror. A conical lens refracts light scattered at some particular angle into a parallel beam which is directed by a mirror to the spectrometer, a stable spherical Fabry-Perot interferometer that acts as a tunable optical filter. The transmission frequencies of the FPS are swept across the scattered light spectrum by density scanning, and the transmitted light is detected by an ITT FW 130 photomultiplier (PMT) and photon counting electronics. The resulting record is the spectrum of the scattered light convolved with the profile of a single transmission peak of the FPS, repeated periodically along the chart as adjacent FPS resonances pass through the scattered light spectrum. The repetition period on the chart serves to calibrate its frequency axis, the period length corresponding to a frequency interval equal to the free spectral range of the FPS.

B. Laser and analyzing interferometer

The light source for these experiments is diagrammed in Fig. 3. Single-mode operation was achieved by means of the Fox-Smith scheme.[23] Initial frequency stabilization was achieved by mounting the apparatus on a vibration isolation table (resonant frequency ~1 Hz). Three servo loops were employed to further stabilize the laser frequency and are indicated in Fig. 3. The fast loop (bandwidth =100 Hz), first proposed by Smith,[24] piezoelectrically varies the main cavity length to lock the laser oscillation frequency to a resonance of the Fox-Smith interferometer, eliminating rapid fluctuations in frequency. An integrating thermal loop adjusts the length of the aluminum structural element of the laser cavity in order to keep the fast loop operating about the

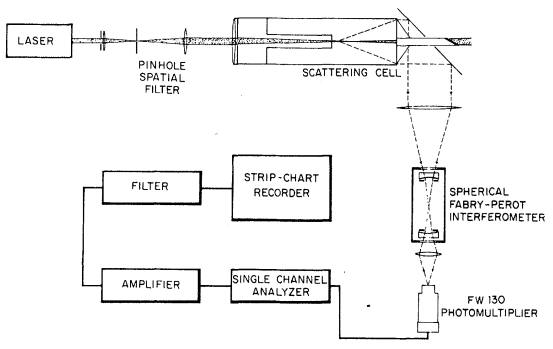

FIG. 2. Experimental apparatus.

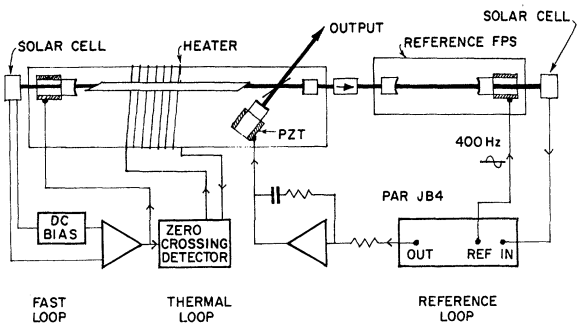

FIG. 3. Laser and associated servo loops.

middle of its dynamic range. Finally a reference loop (bandwidth = 10 Hz) piezoelectrically varies the Fox-Smith cavity length to lock the oscillation frequency to a resonance of an evacuated, thermally stabilized, spherical Fabry-Perot interferometer. This loop employs electronic integration in the feedback circuit to maintain operation at the center of the servo dynamic range in the presence of long-term drift in the length of the Fox-Smith cavity.[25] With the servo loops operating the spectral width of the laser (i.e., the extent of rapid frequency excursions) is $\lesssim$800 KHz.

The interferometer used to frequency-analyze the scattered light was an FPS with the following properties: confocal spacing, 12.997 cm; mirror reflectivity, 96.5%; free spectral range, 576.5 MHz; aperture radius, 2.5 mm; full width at half-height (FWHH), 24 MHz. The FPS mirrors were mounted on an inver tube inside a sealed can. The FPS resonant frequencies were swept in time by varying the gas density and therefore the refractive index of the gas in the can. To reduce frequency drifts of this interferometer the can and scanning device were insulated and temperature controlled to drift less than 0.01°C/h. With these precautions random drifts between the laser and measuring FPS frequencies were reduced to $\lesssim$3 MHz/h. This drift rate produced fractional fluctuations in the spacing between adjacent interferometer orders on the strip chart of ~0.3%. Frequency drifts therefore contribute an error of ~0.3% to the frequency scale factor of the measured spectra.

C. Scattering cell and geometry

Efficient light collection and the elimination of stray light are the prime experimental considerations in the measurement of the spectra of dilute gases. The scattering geometry employed is detailed in Fig. 4. The conical lens was used because of its superior light collection ability when the scattering angle has to be well defined ($\Delta H/H < 10^{-2}$ in this case). A number of steps have been taken to reduce stray light. (i) the conical lens was drilled and fitted with a tube terminated by a Brewster's angle window. (ii) Special care is taken to eliminate stray illumination of surfaces directly viewed by the spectrometer. For instance, stop B shadows the crosshatched region of the cell wall: (iii) The incident laser beam was pinhole spatial filtered to the diffraction limit. (iv) Stray scattering at the surfaces of the focusing lens was eliminated by stops A, B, and C. (v) Dust was millipore filtered out of the cell and did not contribute to the stray light.

With these steps stray light was reduced to an insignificant level. Typical stray-light contributions to observed spectra are shown in Fig. 5. Quantitatively the contribution of stray light to the total observed intensity was $\lesssim$0.05% of that of xenon at STP. The residual stray light entering the spectrometer was probably due to the rather poor condition of the conical lens surface, enhancing the probability for scattering stray light into collected rays. Considerable reduction of the stray-light level reported here should be possible with this design with the employment of micropolished (0/0) surfaces on the key optical elements.

The scattering angle $\Theta = 10.58° \pm 0.018°$ was determined by measuring the deflection of He-Ne

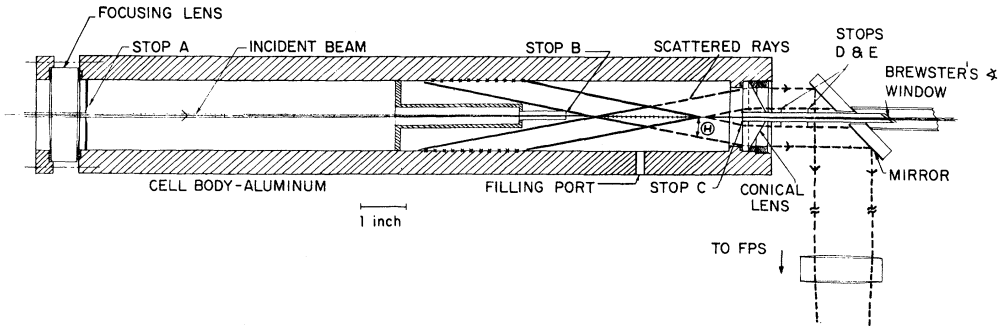

FIG. 4. Scattering cell geometry

laser light by the conical lens. Optical alignment was achieved by maximizing the intensity of the laser beam exiting the scattering cell and the intensity of the collected scattered light. Samples were Matheson research-grade xenon.

D. Data analysis

Data analysis in these experiments involved comparing experimentally measured spectra, $S_e(x,y)$, with the convolutions of theoretical spectra and the instrumental profile. Convolutions were carried out numerically using discrete fast Fourier transform techniques. The instrumental profile of the analyzing interferometer was obtained by scattering light from solutions of polystyrene spheres in water contained in a cell having the same geometry as the gas cell to produce the same light distribution in the FPS. This latter constraint is important since the apertures of the analyzing FPS were chosen large to maximize light collection. With this choice of apertures spherical aberration makes the instrumental profile non-Lorentzian and dependent on the spatial intensity distribution of the scattered light.

The accuracy of convolutions is limited by the choice of the spacing between adjacent data points, Δx, and by the range in x, R_x, covered by the arrays to be convolved. These parameters were selected to yield convolutions accurate to better than 0.01%: $0.025 \geq \Delta x \geq 0.006\,25$, $R_x = 6.4$.

IV. DATA

We have measured the spectrum of He-Ne laser light scattered at an angle of $\Theta = 10.58°$ by pure xenon gas at a temperature $T = 22 \pm 1$°C at sixteen pressures, p, in the range $0.022 \leq p \leq 0.66$ atm. The corresponding range in the uniformity parameter y will be $0.11 \leq y \leq 5.4$, over which the entire kinetic-hydrodynamic transition is mapped out.

Spectra were measured as functions of two parameters: the reduced frequency x and the uniformity parameter y. The reduced frequency x was determined on the data by the frequency calibration. The frequency interval Δf_x corresponding to a unit change in x is obtained from Eq. (2):

$$\Delta f_x \equiv \frac{\sqrt{2}Kv_0}{2\pi} = 2.578\times10^6\left(\frac{T(°\mathrm{K})}{\mathrm{MW}}\right)^{1/2}\frac{\sin\frac{1}{2}\Theta}{\lambda(\mathring{\mathrm{A}})}\ \mathrm{MHz}, \quad (7)$$

where MW is the molecular weight and λ is the wavelength in the gas under study. For our experiments $\Delta f_x = 56.31 \pm 0.15$ MHz, with the error due almost entirely to the error in frequency calibration. The change in Δf_x due to the variation of the refractive index over the pressure range is negligible ($\lesssim 0.01$ MHz).

The uniformity parameter y is given by Eq. (3),

$$y = \frac{\sqrt{2}}{3}\frac{mn_0v_0}{\eta K} = 4.17\times10^{-2}\left[\left(\frac{\mathrm{MW}}{T(°\mathrm{K})}\right)^{1/2}\frac{p(\mathrm{atm})\lambda(\mathring{\mathrm{A}})}{\eta(\mu\mathrm{Poise})\sin\frac{1}{2}\Theta}\right]. \quad (8)$$

Using the measured viscosity of xenon of 228.85 μpoise at $T = 22$°C [19] we find for our experiments:

$$y = (8.326 \pm 0.012)[p(\mathrm{atm})]. \quad (9)$$

Error in the determination of y was due also to error in the pressure measurements varying from ~1% at $p = 0.02$ atm to ~0.1% at $p = 1$ atm.

Typical measured spectra obtained in xenon gas are shown in Fig. 5. The contribution of stray light is determined by evacuating the cell at the end of a run and subtracted out. For comparison with the theory experimental spectra are normalized to unit area in x. Both measured spectra and the instrumental profile are symmetric within experimental error so that the final data from each spectrum is the average of the right and left hand sides. From 4 to 10 measured spectra are averaged to obtain experimental $S_e(x,y)$ for each y.

Kinetic model spectra were numerically convolved with the instrumental profile $I(x)$, to obtain theoretical $S_e(x,y) = S(x,y) \otimes I(x)$, normalized to unit area in x. Experimental spectra for xenon gas have been compared with the results of the kinetic model calculation for both Maxwell and hard-sphere molecules. This comparison involves no adjustable parameters. Since the measurements

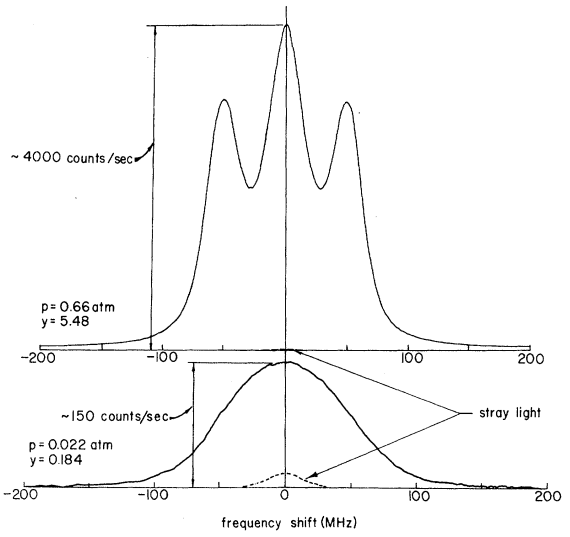

FIG. 5. Typical spectra observed in xenon gas at $T = 22$ °C, $\Theta = 10.58°$.

were made by changing p at constant K the instrumental profile is the same for all values of y. Figure 1 shows $I(x)$, Maxwell molecules spectra $S(x,y)$ calculated from the kinetic model, and the convolved spectra $S_e(x,y)$ for several values of y. The effect of the convolution becomes more serious as y increases and the features of $S(x,y)$ become sharper.

The experimental data are shown plotted in Fig. 6 along with $S_e(x,y)$ from the kinetic model for both Maxwell molecules and hard spheres. The results of the exact hydrodynamic calculation $S_{NS}(x,y) \otimes I(x)$, have also been plotted for selected values of x. Each column of open circles in Fig. 6 represents the experimentally determined spectrum $S_e(x,y)$ at the value of y indicated. The curves presented here show $S_e(x,y)$ as a function of y at various values of frequency shift x. Considering Fig. 1 to be a plot of $S_e(x,y)$ in the x-y plane, the curves of Fig. 6 are obtained by cutting the function $S_e(x,y)$ in planes of constant x. Spectra increase with increasing y in the vicinity of the central line ($x \sim 0$) and Brillouin line ($x \sim 0.9$), and decrease at the intermediate points ($x \sim 0.5$).

The asymptotic limits of the measured spectra for large y ($y = \infty$) and small y ($y = 0$) have been indicated. The $y = 0$ points are determined from the convolution of $I(x)$ with the kinetic limit Gaussian distribution. As y increases the widths of the central and Brillouin lines decrease so the $y \to \infty$ limit $S_e(x,y)$ is $I(x)$ convolved with three properly weighted and spaced δ functions.

We have shown, in Fig. 6 the variation of $S(x,y)$ at $x = 0$ from the kinetic model calculation for Maxwell molecules. This is to indicate the comparative variations of $S(x,y)$ and $S_e(x,y)$ with y. Generally, the convolved spectra $S_e(x,y)$ change more slowly with y than do $S(x,y)$, but in much the same way over the range of y studied.

Random error in the measurement of $S_e(x,y)$ is indicated in Fig. 6 by the fluctuation of the data about smooth functions of y. rms fluctuation $\Delta S_e(x,y)$ in the measurement of a point of $S_e(x,y)$ was typically $\Delta S_e(x,y) < 0.006$, which is the diameter of the open circles. Estimates of net random error arising from shot noise, temperature variation, frequency drift, optical misalignment, and laser linewidth variation are consistent with this value. The rms fluctuation was largest for values of $S_e(x,y)$ with the largest slope in x, e.g., $x = 0.2$, 0.3, 0.6, 0.7 for $y > 1$. The primary source of systematic error $S_e(x,y)$ is the finite distribution of scattering vectors K, arising from the finite dimension of the illuminated region and the finite collection aperture of the analyzing FPS. This distribution leads to a spurious increase in the measured width of the Brillouin peak. For our experimental conditions the Brillouin width of the measured spectrum would be increased by ~0.5% at $y = 6$, ~0.3% at $y = 3$ and ~0.2% at $y = 2$. These errors are small compared to the random error in the measurements and do not substantially alter the data. Since they are difficult to correct for accurately, they were neglected.

V. RESULTS

In Fig. 6, we compare the spectra obtained from the exact solution of the BE for both the Maxwell

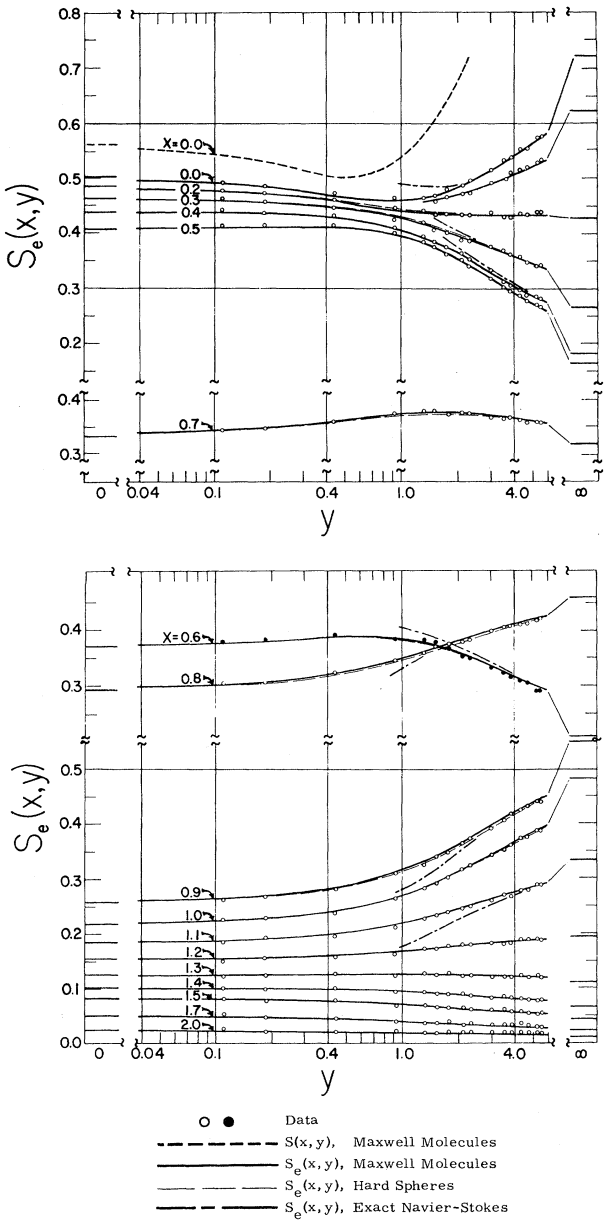

FIG. 6. Comparison of measured and calculated spectra, $S_e(x,y)$, for xenon gas.

and hard-sphere molecules with the measured spectra in xenon gas for $0.1 < y < 5.4$, $T = 22°C$ and $K = 2 \times 10^4$ cm^{-1}. This comparison shows very good agreement for both cases. The measurements do not allow a clear choice between Maxwell and hard-sphere intermolecular potentials.

The agreement indicates that the linearized BE when solved using the converged kinetic model procedure ($M = 21$) accurately provides the density fluctuation spectrum of a dilute monatomic gas. The fact that agreement is obtained for such crude models is evidence of the insensitivity of the density fluctuation spectrum to the form of the intermolecular potential.

We now discuss the applicability of the various hydrodynamic calculations. The measurements presented here establish the exact solution of the BE as an accurate means of calculating the density fluctuation spectrum for a dilute monatomic gas. It would seem appropriate, therefore, to judge the hydrodynamic calculations for a given intermolecular potential on the basis of the agreement of their spectra with those calculated from the exact solution of the BE for the same potential. The various spectra are tabulated in Appendix B. The comparison was made for Maxwell molecules.

As can be seen the agreement between the hydrodynamic and kinetic model calculations improves as y increases and is excellent for $y = 6$. For $y < 3$, however, the breakdwon of hydrodynamics is evident. The spectra calculated from KdM approximation agree with the exact Navier-Stokes spectra to within ~1% for $y > 3$, that is for all values of y for which the hydrodynamic approximation can be considered to be valid. The results of the 3L approximation, however, differ substantially from the Navier-Stokes spectra even when the latter agree well with the kinetic model spectra. The deviation is especially noticeable in the tails ($x > 1$) where the 3L spectra fall off as x^{-2} whereas the KdM and Navier-Stokes spectra have x^{-4} tails. The failure of the 3L spectrum indicates the importance at small y of the asymmetric contributions to the Brillouin peaks which are deleted in going from KdM to the 3L approximation, as has been noted by Lallemand.[5]

The best agreement of the hydrodynamic and BE spectra is provided by the generalized hydrodynamic theory of Selwyn and Oppenheim applied to the Maxwell gas. The agreement for $y = 6$ is excellent, the two calculations differing by <0.1%, and is still quite good at $y = 3$. For smaller y, however, the Selwyn spectrum develops a large peak near $x = 0$.

Selwyn obtained the approximate form $S_{SA}(x, y)$ for his spectrum by expanding the exact spectrum of Eq. (A7), $S_{SE}(x, y)$, in partial fractions and deleting terms of $O(1/y^4)$ or smaller. The approximations are such that $S_{SE}(x, y)$ and $S_{SA}(x, y)$ are the same to order $1/y^4$, the order to which S_{SE} should approximate KM spectra.

The spectra from the Burnett approximation for Maxwell molecules show somewhat better agreement with the kinetic model Maxwell molecule spectra in the vicinity of the sound propagation peaks than the Navier-Stokes spectra. This is an agreement with the measurements of the dispersion relation for forced sound propagation,[27,28] and the light scattering results of Lallemand.[5] The Burnett approximation, however, fails in the central portion of the spectrum, consistently falling low, and thus does not give a clearly better description of $S(x, y)$ than the Navier-Stokes, in contrast with Lallemand's conclusions.[5]

Because of the close relationship between the density fluctuation spectrum and the dispersion relation for forced sound propagation it is of interest to compare the results obtained here with the results of the sound propagation calculations and experiments. Using the kinetic model, Sirovich and Thurber[28] have calculated the dispersion relation for sound propagation for both Maxwell molecules and hard spheres and have compared their calculations with the measurements of Greenspan[26] and Meyer and Sessler.[29] Buckner and Ferziger[30] have also calculated dispersion relations for sound in a Maxwell gas. Their results have been tested by Schotter.[31] Over the range y of interest here, $0.1 < y < 5.4$, the calculated Maxwell molecule and hard-sphere dispersion relations are somewhat different with the Maxwell calculation showing good agreement with the measurements. However, the calculated dispersion relations for Maxwell and hard-sphere molecules show more difference than expected on the basis of a comparison of the calculated Maxwell and hard-sphere spectra, probably because the kinetic model approximation was carried out only to order $M = 11$ in the calculations of Sirovich and Thurber. Sugawara, Yip, and Sirovich[16] show that it is necessary to carry the kinetic model calculation to $M = 21$ for the hard-sphere gas to obtain sufficient convergence in the calculation of the spectra. One would expect the same kind of behavior for the dispersion relation. It may be, then, that some of the difference observed between the measured dispersion relation and the hard sphere calculation of the dispersion relation of Sirovich and Thurber is due to a lack of convergence.

Of particular interest is the comparison of forced sound data and hydrodynamic calculations for Maxwell molecules. Using the results of Foch and Uhlenbeck[27] and Selwyn and Oppenheim[13] it is evident that at large y for Maxwell molecules both

Burnett hydrodynamics and generalized hydrodynamics produce the same dispersive corrections to the forced sound dispersion relations as does the kinetic model. As we have just noted, the corrections to sound speed and attenuation predicted by these theories have been shown to work well. However, because they all predict the same results, it is not possible to distinguish among them using forced sound. The density fluctuation spectra, on the other hand, show generalized hydrodynamics to be superior to the Burnett in approximating the kinetic model spectra.

Comparison of Eqs. (A8) and (A4) shows that the first corrections to the spectral features (peak amplitudes, locations, and widths) of the asymptotic three Lorentzian form calculated from generalized hydrodynamics are of order $1/y^2$. If these are the proper corrections then differences between kinetic model and generalized hydrodynamic features should be $\lesssim 1/y^4$. This condition is in fact satisfied.

On the other hand, although first corrections in the Burnett spectra are also of order $1/y^2$, differences between Burnett and kinetic model features are of order $1/y^3$. The lowest-order corrections to spectral features in the Burnett approximation are therefore not correct.

VI. SUMMARY

Our main result has been to show that density fluctuation spectra obtained from the kinetic model solution of the Boltzmann equation for a gas of Maxwell or hard-sphere molecules agree well with measured spectra in dilute xenon. Having extablished this we compare various hydrodynamic and kinetic model calculations for a Maxwell gas. This comparison shows the superiority of generalized hydrodynamics in describing asymptotic deviations from Navier-Stokes hydrodynamics.

ACKNOWLEDGMENTS

Among the many people who have helped during the course of this work, I would especially like to thank G. B. Benedek for his guidance and criticism, T. J. Greytak and the late J. H. Lunacek for their many ideas and suggestions, and S. Yip for his continued interest and encouragement.

APPENDIX A

In this Appendix we collect the formulas used to calculate the hydrodynamic density fluctuation spectra, $S(x,y)$ discussed in the main text. Equations 2–4 were used with the Eucken ratio taken to have the Maxwell value of 2.50. Spectra are normalized to unit area in x. Comparison with kinetic model spectra is made in Appendix B.

With the following notation: Exact Navier-Stokes,[10] $S_{NS}(x,y)$; Kadanoff-Martin,[11] $S_{KdM}(x,y)$; three Lorentzians,[10] $S_{3L}(x,y)$; Burnett,[12] $S_B(x,y)$; Selwyn exact,[13] $S_{SE}(x,y)$; Selwyn approximate,[13] $S_{SA}(x,y)$; we have

$$S_{NS}(x,y)=\frac{1}{\pi}\,\mathrm{Re}\left(\begin{vmatrix}1 & 1 & 0\\ 0 & ix+4/9y & -\frac{1}{2}\\ 0 & \frac{2}{3} & ix+5/6y\end{vmatrix}\Bigg/\begin{vmatrix}ix & 1 & 0\\ -\frac{1}{2} & ix+4/9y & -\frac{1}{2}\\ 0 & \frac{2}{3} & ix+5/6y\end{vmatrix}\right), \tag{A1}$$

$$S_{NS}(x,y)=\frac{1}{\pi}\,\mathrm{Re}\frac{-x^2+ix(23/18y)+20/54y^2+\frac{1}{3}}{-ix^3-x^2(23/18y)+ix[\frac{5}{6}+(20/54y^2)]+5/12y}, \tag{A2}$$

$$S_{KdM}(x,y)=\frac{1}{5\pi y[x^2+(1/2y)^2]}+\frac{1}{10\pi y}\left(\frac{\frac{50}{9}-2x^2}{(x^2-\frac{5}{6})^2+(7x/9y)^2}\right), \tag{A3}$$

$$S_{3L}(x,y)=\frac{1}{5\pi y[x^2+(1/2y)^2]}+\frac{10.5}{90\pi y}\left\{\left[(x+\sqrt{\tfrac{5}{6}})^2+\left(\frac{7}{18y}\right)^2\right]^{-1}+\left[(x-\sqrt{\tfrac{5}{6}})^2+\left(\frac{7}{18y}\right)^2\right]^{-1}\right\}, \tag{A4}$$

$$S_B(x,y)=\frac{1}{\pi}\,\mathrm{Re}\left(\begin{vmatrix}1 & 1 & 0\\ 0 & ix+4/9y & -\frac{1}{2}+4/54y^2\\ 0 & \frac{2}{3}+14/54y^2 & ix+5/6y\end{vmatrix}\Bigg/\begin{vmatrix}ix & 1 & 0\\ -\frac{1}{2}-16/54y^2 & ix+4/9y & -\frac{1}{2}+4/54y^2\\ 0 & \frac{2}{3}+14/54y^2 & ix+5/6y\end{vmatrix}\right), \tag{A5}$$

$$S_B(x,y)=\frac{1}{\pi}\,\mathrm{Re}\left(\frac{-x^2+ix(23/18y)+(1/y^2)(73/162-14/729y^2)+\frac{1}{3}}{-ix^3-x^2(23/18y)+ix(\frac{5}{6}+121/162y^2-14/729y^4)+5/12y+20/81y^3}\right), \tag{A6}$$

$$S_{SE}(x,y)=(1/\pi)\,\mathrm{Re}(N/D), \tag{A7}$$

where

$$N = -x^2 + ix(\tfrac{23}{12}y + 1.5ix)Z_1Z_2 + \tfrac{1}{3} + \tfrac{1}{9}Z_1Z_2 - ix\left(\frac{.27Z_2^2}{5(ix+\frac{9}{4}y)} + \tfrac{8}{5}Z_1Z_2^2 + 5Z_1^3 + 2Z_1^2Z_2 + \frac{7Z_1^2}{(ix+\frac{7}{4}y)}\right),$$

$$D = -ix^3 - x^2(\tfrac{23}{12}y + 1.5ix)Z_1Z_2 + ix(\tfrac{5}{6} + \tfrac{1}{9}Z_1Z_2) + \tfrac{1}{9}x^2\left(\frac{27Z_2^2}{5(ix+\frac{9}{4}y)} + \tfrac{8}{5}Z_1Z_2^2 + 5Z_1^3 + 2Z_1^2Z_2 + \frac{7Z_1^2}{(ix+\frac{7}{4}y)}\right)$$

$$+ \tfrac{5}{12}Z_1 - \tfrac{1}{18}Z_1^2\left(5Z_1 + 2Z_2 + \frac{7}{(ix+\frac{7}{4}y)}\right),$$

$$Z_1 = (ix+y)^{-1}, \quad Z_2 = (ix+1.5y)^{-1};$$

$$S_{SA}(x,y) = \frac{1}{\pi}\,\mathrm{Re}\left(\frac{A}{ix+\gamma_1} + \frac{B-iC}{i(x-x')+\gamma_2} + \frac{B+iC}{i(x+x')+\gamma_2}\right), \tag{A8}$$

where

$$A = \tfrac{2}{5} + 1/25y^2, \quad B = \tfrac{3}{10} - 1/50y^2, \quad C = \sqrt{\tfrac{5}{6}}\,[\tfrac{13}{20} - (\tfrac{251}{2160})(1/y^2)],$$

$$x' = \tfrac{5}{6}[1 + \tfrac{19}{540}(1/y^2)], \quad \gamma_1 = (1/2y)[1 - 1/2y^2], \quad \gamma_2 = (7/18y)[1 - \tfrac{53}{189}(1/y^2)].$$

APPENDIX B

In Table II, density fluctuation spectra $S(x,y)$, calculated from the kinetic and hydrodynamic theories discussed in this paper, are tabulated for selected x,y values. Spectra are normalized to unit area in x. Table III gives the Brillouin peak height and location for the various spectra.

TABLE II. Comparison of kinetic model spectra and hydrodynamic spectra.

	Kinetic model			Navier-Stokes			Selwyn	
x	Maxwell	Hard spheres	Exact	Kadanoff-Martin	3 Lorentzians	Burnett	Exact	Approx.
				$y = 0.767$				
0.0	0.5151	0.5162	0.5642	0.5273	0.2841	0.3047		
0.1	0.5046	0.5069	0.5611	0.5247	0.2813	0.3048		
0.2	0.4793	0.4837	0.5523	0.5174	0.2742	0.3057		
0.3	0.4517	0.4569	0.5390	0.5070	0.2657	0.3083		
0.4	0.4311	0.4348	0.5206	0.4935	0.2594	0.3138		
0.5	0.4205	0.4207	0.4938	0.4742	0.2577	0.3238		
0.6	0.4168	0.4127	0.4527	0.4434	0.2612	0.3388		
0.7	0.4140	0.4045	0.3932	0.3961	0.2678	0.3598		
0.8	0.3982	0.3850	0.3190	0.3331	0.2726	0.3790		
0.9	0.3499	0.3430	0.2424	0.2632	0.2691	0.3918		
1.0	0.2776	0.2779	0.1754	0.1980	0.2535	0.3833		
1.1	0.2003	0.2041	0.1238	0.1446	0.2278	0.3430		
1.2	0.1348	0.1392	0.0869	0.1046	0.1974	0.2803	0.0816	
1.3	0.0881	0.0912	0.0614	0.0758	0.1676	0.2115	0.0645	
1.4	0.0574	0.0591	0.0440	0.0555	0.1414	0.1528	0.0518	
1.5	0.0376	0.0384	0.0321	0.0412	0.1194	0.1088	0.0407	
2.0	0.0059	0.0056	0.0085	0.0116	0.0580	0.0238	0.0072	
2.5	0.0012	0.0012	0.0031	0.0044	0.0339	0.0077	0.0013	
3.0	0.0004	0.0004	0.0014	0.0020	0.0224	0.0032	0.0003	
				$y = 1.312$				
0.0	0.5700	0.5636	0.5498	0.5282	0.3956	0.4389	1.8900	0.6507
0.1	0.5347	0.5342	0.5304	0.5097	0.3758	0.4255	0.4994	0.5930
0.2	0.4624	0.4701	0.4869	0.4684	0.3308	0.3945	0.2351	0.4840
0.3	0.4007	0.4095	0.4448	0.4395	0.2855	0.3628	0.1911	0.3983
0.4	0.3667	0.3730	0.4202	0.4082	0.2553	0.3426	0.2017	0.3520
0.5	0.3607	0.3625	0.4180	0.4093	0.2459	0.3394	0.2502	0.3403
0.6	0.3802	0.3756	0.4359	0.4307	0.2603	0.3578	0.3577	0.3611

Table II *(Continued)*

	Kinetic model			Navier-Stokes			Selwyn	
x	Maxwell	Hard spheres	Exact	Kadanoff-Martin	3 Lorentzians	Burnett	Exact	Approx.
				$y=1.312$				
0.7	0.4213	0.4100	0.4591	0.4591	0.2995	0.3934	0.5120	0.4055
0.8	0.4616	0.4467	0.4492	0.4573	0.3525	0.4431	0.6364	0.4626
0.9	0.4443	0.4369	0.3696	0.3856	0.3807	0.4692	0.5125	0.4657
1.0	0.3374	0.3418	0.2525	0.2698	0.3465	0.4152	0.3036	0.3567
1.1	0.2100	0.2169	0.1562	0.1699	0.2730	0.2953	0.1718	0.2154
1.2	0.1221	0.1264	0.0952	0.1049	0.2030	0.1847	0.1017	0.1197
1.3	0.0719	0.0735	0.0596	0.0662	0.1512	0.1127	0.0634	0.0671
1.4	0.0439	0.0440	0.0387	0.0433	0.1153	0.0703	0.0410	0.0390
1.5	0.0278	0.0288	0.0262	0.0294	0.0905	0.0457	0.0275	0.0234
2.0	0.0046	0.0043	0.0057	0.0065	0.0373	0.0088	0.0048	0.0022
2.5	0.0012	0.0010	0.0019	0.0022	0.0209	0.0028	0.0012	0.0004
3.0	0.0004	0.0003	0.0008	0.0010	0.0135	0.0012	0.0004	0.0007
				$y=3.00$				
0.0	0.8895	0.8763	0.8583	0.8488	0.7931	0.8239	0.9243	0.8986
0.1	0.6611	0.6630	0.6560	0.6483	0.5919	0.6339	0.6679	0.6649
0.2	0.3997	0.4070	0.4098	0.4050	0.3465	0.3982	0.3922	0.4000
0.3	0.2736	0.2793	0.2852	0.2823	0.2220	0.2776	0.2657	0.2731
0.4	0.2231	0.2273	0.2345	0.2327	0.1644	0.2256	0.2164	0.2223
0.5	0.2151	0.2173	0.2278	0.2266	0.1486	0.2162	0.2095	0.2142
0.6	0.2454	0.2446	0.2622	0.2614	0.1680	0.2434	0.2406	0.2441
0.7	0.3366	0.3303	0.3636	0.3629	0.2450	0.3278	0.3335	0.3345
0.8	0.5565	0.5415	0.5964	0.5961	0.4550	0.5309	0.5597	0.5526
0.9	0.8087	0.7945	0.7776	0.7847	0.7585	0.8017	0.8223	0.8087
1.0	0.4652	0.4758	0.4089	0.4178	0.5314	0.5125	0.4639	0.4683
1.1	0.1794	0.1816	0.1622	0.1662	0.2591	0.2024	0.1776	0.1806
1.2	0.0789	0.0794	0.0737	0.0755	0.1419	0.0887	0.0780	0.0791
1.3	0.0403	0.0402	0.0386	0.0396	0.0892	0.0452	0.0399	0.0403
1.4	0.0230	0.0226	0.0225	0.0231	0.0617	0.0258	0.0228	0.0229
1.5	0.0142	0.0143	0.0141	0.0145	0.0457	0.0160	0.0141	0.0141
2.0	0.0024	0.0024	0.0027	0.0027	0.0171	0.0029	0.0025	0.0024
2.5	0.0008	0.0008	0.0009	0.0009	0.0093	0.0009	0.0007	0.0007
3.0	0.0003	0.0003	0.0004	0.0004	0.0060	0.0004	0.0003	0.0002
				$y=6.00$				
0.0	1.5978	1.5799	1.5750	1.5703	1.5427	1.5595	1.5985	1.5956
0.1	0.6688	0.6729	0.6719	0.6695	0.6415	0.6681	0.6685	0.6690
0.2	0.2693	0.2730	0.2731	0.2721	0.2431	0.2717	0.2694	0.2699
0.3	0.1589	0.1613	0.1614	0.1610	0.1299	0.1603	0.1589	0.1592
0.4	0.1226	0.1235	0.1247	0.1245	0.0903	0.1236	0.1226	0.1229
0.5	0.1171	0.1180	0.1193	0.1192	0.0798	0.1176	0.1171	0.1173
0.6	0.1374	0.1387	0.1405	0.1404	0.0922	0.1375	0.1375	0.1376
0.7	0.2080	0.2088	0.2140	0.2138	0.1487	0.2064	0.2078	0.2080
0.8	0.4679	0.4638	0.4883	0.4877	0.3839	0.4589	0.4681	0.4680
0.9	1.4827	1.4625	1.4862	1.4879	1.4323	1.4614	1.4807	1.4787
1.0	0.4549	0.4623	0.4303	0.4336	0.5371	0.4752	0.4544	0.4549
1.1	0.1139	0.1143	0.1105	0.1113	0.1681	0.1183	0.1140	0.1141
1.2	0.0440	0.0438	0.0432	0.0435	0.0802	0.0455	0.0441	0.0441
1.3	0.0214	0.0217	0.0213	0.0214	0.0477	0.0222	0.0215	0.0215
1.4	0.0121	0.0120	0.0120	0.0121	0.0322	0.0124	0.0120	0.0120
1.5	0.0074	0.0074	0.0074	0.0074	0.0235	0.0076	0.0074	0.0074
2.0	0.0013	0.0013	0.0014	0.0014	0.0086	0.0014	0.0013	0.0013
2.5	0.0004	0.0004	0.0004	0.0004	0.0047	0.0005	0.0004	0.0004
3.0	0.0002	0.0002	0.0002	0.0002	0.0030	0.0002	0.0002	0.0002

TABLE III. Brillouin peak height and location for kinetic model and hydrodynamic spectra.

y		Height	Location	y		Height	Location
1.312	Maxwell	0.463	0.821	4.65	Maxwell	1.193	0.907
	Hard spheres	0.451	0.837		Hard spheres		
	NS exact	0.462	0.735		NS exact	1.174	0.902
	NS KdM	0.465	0.750		NS KdM	1.178	0.902
	NS 3L	0.381	0.900		NS 3L	1.160	0.913
	B	0.469	0.894		B	1.186	0.910
	SWN exact	0.637	0.803		SWN exact	1.193	0.907
	SWN approx.	0.477	0.856		SWN approx.	1.189	0.907
3.00	Maxwell	0.810	0.900	6.00	Maxwell	1.503	0.909
	Hard spheres	0.800	0.906		Hard spheres	1.503	0.910
	NS exact	0.788	0.884		NS exact	1.498	0.907
	NS KdM	0.793	0.885		NS KdM	1.501	0.906
	NS 3L	0.765	0.913		NS 3L	1.488	0.913
	B	0.804	0.907		B	1.508	0.910
	SWN exact	0.822	0.897		SWN exact	1.505	0.909
	SWN approx.	0.809	0.900		SWN approx.	1.506	0.909

*This work was supported by the Center for Materials Science and Engineering of the Massachusetts Institute of Technology and by NSF Grants DMR 7302020 and DMR 7302088 with the Division of Engineering and Applied Physics, Harvard University.

[1]M. Nelkin and A. Ghatak, Phys. Rev. 135, A4 (1964).
[2]M. Nelkin and S. Yip, Phys. Fluids 9, 380 (1966).
[3]T. J. Greytak and G. B. Benedek, Phys. Rev. Lett. 17, 179 (1966).
[4]A. D. May, E. G. Rawson, and H. L. Welsh, in *Physics of Quantum Electronics*, edited by P. L. Kelley, B. Lax, and P. E. Tannenwald (McGraw-Hill, New York, 1966), p. 260.
[5]P. Lallemand, J. Phys. (Paris) 31, 551 (1970).
[6]This paper is based on the author's Ph.d. thesis (Massachusetts Institute of Technology, 1970) (unpublished).
[7]L. I. Komarov and I. Z. Fisher, Zh. Eksp. Teor. Fiz. 43, 1927 (1962) [Sov. Phys.—JETP 16, 1358 (1963)].
[8]A. Sugawara, S. Yip, and L. Sirovich, Phys. Rev. 168, 121 (1968).
[9]The kinetic-hydrodynamic transition was first described by L. D. Landau and G. Placzek, Phys. Z. Sowjetunion 5, 172 (1934). See also *Collected Papers of L. D. Landau* (Gordon and Breach, London, 1965), p. 79.
[10]R. D. Mountain, Rev. Mod. Phys. 38, 205 (1966). L. D. Landau and E. M. Lifshitz, *Fluid Mechanics* (Addison Wesley, New York, 1959), Sec. 77.
[11]L. P. Kadanoff and P. C. Martin, Ann. Phys. (N.Y.) 24, 419 (1963).
[12]S. Ranganathan and M. Nelkin, Phys. Fluids 10, 2085 (1967).
[13]P. A. Selwyn and I. Oppenheim, Physica 54, 161, 195 (1971).
[14]J. M. J. Van Leeuwen and S. Yip, Phys. Rev. 139, A1138 (1965).
[15]S. Yip and M. Nelkin, Phys. Rev. 135, A1241 (1964). S. Yip and S. Ranganathan, Phys. Fluids 8, 1956 (1965). S. Ranganathan and S. Yip, Phys. Fluids 9, 372 (1966).
[16]A. Sugawara, S. Yip, and L. Sirovich, Phys. Fluids 11, 925 (1968). We are indebted to S. Yip for the computer programs used in calculating kinetic model spectra.
[17]E. P. Gross and E. Jackson, Phys. Fluids 2, 432 (1965).
[18]G. E. Uhlenbeck and G. W. Ford, *Lectures in Statistical Mechanics* (American Mathematical Society, Providence, R. I., 1963), Chap. 6.
[19]J. Kestin and W. Liedenfrost, Physica 25, 1033 (1959).
[20]F. G. Keyes, Trans. Am. Soc. Mech. Eng. 76, 809 (1954); 77, 1395 (1955); W. G. Kannuluik and E. H. Carmen, Proc. Phys. Soc. Lond. B 65, 701 (1952); S. C. Saxena, Indian J. Phys. 31, 597 (1957); B. N. Srivastava and S. C. Saxena, Proc. Phys. Soc. B 70, 369 (1957); H. Ziebland and J. T. A. Burton, Br. J. Appl. Phys. 39, 51 (1968); H. L. Burge and L. B. Robinson, J. Appl. Phys. 39, 51 (1968); A. A. Tarzimanov, Fiz. Inzhen. Zh. 4 (9) 86, (1961); *CRC Handbook*, 50th ed., (Chemical Rubber Co., Cleveland, 1969), p. E2; *American Institute of Physics Handbook*, 2nd ed., (McGraw-Hill, New York, 1963), Sec. 4, p. 81.
[21]M. W. Zemansky, *Heat and Thermodynamics*, (McGraw-Hill, New York, 1957), 4th ed., p. 122.
[22]J. O. Hirschfelder, C. F. Curtis, and R. B. Bird, *The Molecular Theory of Gases and Liquids* (Wiley, New York, 1954), Chap. 3, Appendix B.
[23]P. W. Smith, IEEE J. Quantum Electron. QE-1, 343 (1965).
[24]P. W. Smith, IEEE J. Quantum Electron. QE-2, 666 (1966).
[25]This technique has also been discussed by S. K. Gordon and S. F. Jacobs, Appl. Opt. 13, 231 (1974).
[26]M. Greenspan, J. Acoust. Soc. Am. 28, 644 (1956).
[27]J. Foch and G. E. Uhlenbeck, Phys. Rev. Lett. 19, 1025 (1967).
[28]L. Sirovich and J. K. Thurber, J. Acoust. Soc. Am. 38, 478 (1965). The uniformity parameter r used in this paper and in Ref. 26 is related to our parameter y by $r=0.164y$.
[29]E. Meyer and G. Sessler, Z. Phys. 149, 15 (1957).
[30]J. K. Buckner and J. H. Ferziger, Phys. Fluids 9, 2315 (1966).
[31]R. Schotter, Phys. Fluids 17, 1163 (1974).